Bauxite Residue Alkali-Magnetization Reduction Roasting Process

Yafei Qi[1] , Xiaolin Pan[2], Haozhuo Zheng[3], Zhicheng Zhang[4] and Haiyan Yu[5]
1, 3. PhD student
2, 5. Professor, Doctoral Supervisor
4. Postgraduate student
Northeastern University - Key Laboratory of Ecological Metallurgy of Multi-metal Symbiotic Minerals of the Ministry of Education
School of Metallurgy of Northeast University
Shenyang Key Laboratory for Recycling and Utilization of Nonferrous Metal Resources
Shenyang, China
Corresponding author: panxl@smm.neu.edu.cn, yuhy@smm.neu.edu.cn
https://doi.org/10.71659/icsoba2025-br011

Abstract

High-iron bauxite residue is a secondary metallurgical resource with complex intergrowth of iron and alumina minerals, making it difficult to recover valuable elements through conventional mineral processing. This study investigates the mineral phase transformation and recovery behaviour of iron and alumina from high-iron bauxite residue under different roasting conditions and reagent formulations, using a 'soda-magnetization reduction roasting' process. The test results indicate that increasing the roasting temperature and NaOH dosage promoted the conversion of $Na_{1.75}Al_{1.75}Si_{0.25}O_4$ to $Na_{1.95}Al_{1.95}Si_{0.05}O_4$, thereby enhancing the leaching rate of alumina. However, excessive NaOH and reductant addition led to the transformation of Fe_3O_4 into $NaFe_{0.75}Al_{0.25}O_2$ and FeO, resulting in a significant decrease in iron recovery. Under optimal conditions, the recovery rates of alumina and sodium oxide in the roasted product reached 81.56 and 90.97 %, respectively. The iron concentrate obtained from magnetic separation had a grade exceeding 55 %, an alumina impurity content below 4 %, and an iron recovery rate above 90 %. The comprehensive reduction rate of high-iron bauxite residue reached 93 %.

Keywords: Bauxite residue, Magnetization roasting, Mineral phase transformation, Alumina leaching, Iron recovery.

1. Background

Bauxite residue is a soda-rich solid waste generated during the Bayer process for alumina production. Approximately 0.8–1.5 tonne of bauxite residue are discharged per tonne of alumina produced. As of 2024, China's alumina output reached 85.5 million tonnes, resulting in a bauxite residue production of 115 million tonnes, with total accumulated stockpiles exceeding 1.6 billion tonnes. However, the comprehensive utilization rate of bauxite residue remains only 12 % [1, 2]. Consequently, most bauxite residue is disposed of in solid waste landfills, leading to loss of land resources and the potential for contamination of groundwater and soil. Effective reduction of bauxite residue is urgently needed, yet progress has been hindered by its complex physicochemical properties. Bauxite residue contains valuable resources such as Fe_2O_3, Al_2O_3, SiO_2, TiO_2, Na_2O, and rare metals, making it promising for comprehensive utilization, particularly for its iron and alumina resources [3−5].

The methods for recovering iron and alumina resources from bauxite residue can be classified into physical beneficiation, hydrometallurgy, and pyrometallurgy processes. However, due to the fine particle size and lattice substitution between iron and aluminium oxides, it is difficult to separate valuable elements from bauxite residue using conventional physical methods. Liu et al.

[6] designed a parabolic hydrocyclone to address the issue of low iron recovery efficiency. The results demonstrated that the parabolic hydrocyclone significantly enhanced the concentration of iron minerals, increasing the iron concentrate grade from 26.75 to 36.04 %. However, this method still faces challenges such as low recovery efficiency and poor concentrate quality, failing to fundamentally achieve effective resource recovery. Zhu et al. [7] treated bauxite residue through acid leaching, extraction, polymerization, soda leaching, and aging processes. This process achieved recovery rates of over 96 % for scandium and vanadium, while more than 97 % of iron and alumina were precipitated and recovered in the form of polymers. Additionally, by-products included a titanium-rich residue with a grade of 62 % and white carbon black with a purity of 99.5 %. Although the acid method demonstrates high efficiency in bauxite residue treatment, its complex process flow and potential risks to reactors [8, 9] hinder its large-scale industrial application for bauxite residue solid waste disposal.

Pyrometallurgy is the most promising method for large-scale resource utilization of bauxite residue, which can be divided into reduction smelting and reduction roasting [10–12]. Reduction smelting involves adding reductants and limestone to reduce iron oxides in bauxite residue into molten iron or pig iron while generating highly reactive calcium aluminate residue that enables alumina recovery. Wu et al. [13] utilized a mixture of steel slag, high-iron bauxite, coal fly ash, and bauxite residue to produce pig iron and smelting slag. The slag contained compounds such as $12CaO \cdot 7Al_2O_3$ and $CaO \cdot Al_2O_3$, which could react with sodium carbonate liquor to recover alumina. Although reduction smelting enables comprehensive recovery of valuable metals from bauxite residue, this process typically requires temperatures exceeding 1400 °C, posing challenges such as high energy consumption, excessive reductant usage, and large residue volumes. The reduction roasting can be divided into metallization and magnetization reduction roasting. In metallization reduction roasting, sodium and calcium salts are used as mineralizers to inhibit the formation of intermediate products during iron metallization reactions, while generating soluble sodium aluminate to recover alumina from bauxite residue. Silicon and titanium oxides in the bauxite residue are simultaneously converted into calcium salts to ensure efficient leaching of sodium aluminate. However, this process still requires a reduction sintering temperature of approximately 1200 °C, and its high energy consumption and high residue volume diminish the economic benefits of the process and limit its industrial application. Therefore, the industry has proposed the magnetization roasting process to reduce energy consumption and improve the efficiency of bauxite residue treatment. The principle involves the targeted conversion of hematite and goethite into magnetite, followed by magnetic separation to recover iron concentrate. The aluminium-, silicon-, and titanium-bearing minerals in bauxite residue lack magnetism and can thus be separated and concentrated in the iron-removed tailings. The magnetization roasting process has been widely applied in the removal of impurities and upgrading of low-grade iron resources. However, due to the lattice substitution of iron and aluminium elements in bauxite residue, the iron concentrate derived from bauxite residue through this method often contains high levels of alumina (Al_2O_3) and sodium oxide (Na_2O), making it difficult to be directly used as raw material for blast furnace ironmaking. Additionally, gibbsite and boehmite in bauxite residue are prone to transform into γ-Al_2O_3 during roasting, leading to a decline in digestion efficiency. This complicates the recovery of alumina resources and results in poor economic viability of the process [14, 15].

Based on the advantages and disadvantages of metallization reduction and magnetization roasting, this study proposes a low-temperature reduction roasting process for recovering iron and alumina from bauxite residue, which includes soda-enhanced magnetization roasting, atmospheric soda leaching, and weak magnetic separation. This study is dedicated to significantly reducing bauxite residue volume and efficiently recovering iron and alumina resources from bauxite residue at relatively low temperatures. It investigates the mineral phase transformation behaviour of roasted products under different roasting and batching ratio conditions, while exploring the recovery

mechanisms of iron and alumina. An efficient, environmentally friendly, and economically viable method for industrial-scale bauxite residue treatment is provided, offering substantial economic and social benefits.

2. Experimental Method

The bauxite residue and soda liquor used in this study were obtained from alumina refineries in Guangxi and Shanxi, respectively, and the coal fly ash was sourced from a coal plant in Liaoning. The solid samples were dried in an oven at 105 °C until constant weight was achieved and then crushed to a particle size below 74 μm for further use. The composition of the bauxite residue is presented in Table 1, with Fe_2O_3 and Al_2O_3 being the major valuable metal components, accounting for 55.64 % and 17.90 %, respectively. Other components included TiO_2 (5.38 %), SiO_2 (4.80 %), CaO (2.40 %), and Na_2O (1.89 %). The reductant, coal fly ash, had fixed carbon and volatile matter contents of 60.40 % and 27.04 %, respectively.

Table 1. Chemical composition of bauxite residue (wt.%).

Fe_2O_3	FeO	Al_2O_3	TiO_2	SiO_2	CaO	Na_2O	MISC.	LOI
55.64	< 0.01	17.90	5.38	4.80	2.40	1.89	2.40	9.58

First, the dried and crushed bauxite residue was dry-mixed with coal fly ash at a certain ratio. Subsequently, the raw mixture was granulated with soda liquor and distilled water to produce moist pellets with a particle size of 3 ± 0.3 cm, which were then dried in an oven to constant weight. The raw pellets were placed in a corundum crucible, and the crucible was inserted into a quartz tube of a tubular furnace filled with argon atmosphere. Both the material and the tubular furnace were heated to the target temperature at a rate of 10 °C/min and held for a specified duration, followed by cooling to room temperature under protective atmosphere along with the furnace.

The obtained reduction product was crushed and then subjected to leaching in a constant-temperature water bath at 85 °C for 15 minutes. The leaching solution consisted of a diluted soda liquor with NaOH concentration of 15 g/L and Na_2CO_3 concentration of 5 g/L. After leaching, the alumina-extracted residue was filtered using a Buchner funnel and repeatedly washed with hot water until neutral. The dried alumina-extracted residue was then separated into iron concentrate and iron-extracted tailings via low-intensity magnetic separation using a magnetic tube. The magnetic separation products were dried in an oven to constant weight, and their mass and chemical composition were determined.

The chemical and mineral compositions of the solid samples were determined by XRF (Rigaku ZSX 100e, Japan) and XRD (Philips X'Pert PW3040-60, Netherlands), respectively. The particle size distribution was measured using a laser particle size analyser (Mastersizer 2000, Malvern, UK). The changes in surface elemental valence states were analysed by X-ray photoelectron spectroscopy analyser (XPS, ESCALAB 250Xi, USA). The Mössbauer spectrum was measured at room temperature using a spectrometer (MFD-500AV-03, Japan) with a $^{57}Co/Rh$ radioactive source and α-Fe^0 as the reference. The micromorphology and elemental distribution of the solid samples were characterized by scanning electron microscopy and energy-dispersive spectroscopy (SEM-EDS, Zeiss Gemini 300, Germany).

The recovery rates of the roasting products Al_2O_3 and Na_2O are calculated using Equations (1) and (2):

$$\eta_{Na_2O} = \frac{(N_0/F_0)-(N_1/F_1)}{(N_0/F_0)} \times 100\ \% \quad (1)$$

$$\eta_{Al_2O_3} = \frac{(A_0/F_0)-(A_1/F_1)}{(A_0/F_0)} \times 100\ \% \quad (2)$$

where
N_0, A_0, F_0 Na_2O, Al_2O_3, and TFe contents (%) in the roasted products,
N_1, A_1, F_1 Na_2O, Al_2O_3, and TFe contents (%) in the alumina-extracted residue.

The yield and iron recovery rate of iron concentrate obtained from magnetic separation of alumina-extracted residue are calculated using Equations (3) and (4):

$$y_{Fe} = \frac{m_2}{m_1} \times 100\ \% \quad (3)$$

$$\varepsilon_{Fe} = \frac{F_2}{F_1} \times y_{Fe} \times 100\ \% \quad (4)$$

where
m_1, m_2 mass of the alumina-extracted residue and iron concentrate, g
F_1, F_2 TFe content of the alumina-extracted residue and iron concentrate, %

3. Results and Discussion

3.1 Influence of Roasting Conditions on Mineral Phase Transformation and Recovery Performance of Valuable Elements

As the most critical parameter in magnetization roasting, the influence of roasting temperature and duration on the mineral phase evolution of the sintered products was first investigated, with the roasting time fixed at 60 min, C/O and N/A molar ratios set at 0.2 and 1.4, respectively, and a magnetic field intensity of 2200 Oe. As shown in Figure 1a and 1b, the roasted products mainly consist of $Na_{1.95}Al_{1.95}Si_{0.05}O_4$, $Na_{1.75}Al_{1.75}Si_{0.25}O_4$, Fe_3O_4, SiO_2, and $CaTiO_3$. The content of $Na_{1.75}Al_{1.75}Si_{0.25}O_4$ in the roasted product decreased from 33.4 to 8.6 %, while that of $Na_{1.95}Al_{1.95}Si_{0.05}O_4$ increased from 6.4 to 32.1 %. When the temperature was raised from 750 to 800 °C, the content of $Na_{1.95}Al_{1.95}Si_{0.05}O_4$ dropped to 21.9 %, the diffraction peak of SiO_2 disappeared, and the content of $Na_{1.75}Al_{1.75}Si_{0.25}O_4$ increased to 17.5 %. These results indicate that higher roasting temperatures favour the conversion of $Na_{1.75}Al_{1.75}Si_{0.25}O_4$ into $Na_{1.95}Al_{1.95}Si_{0.05}O_4$. However, when the temperature reaches 800 °C, SiO_2 participates in the transformation reaction of sodium aluminosilicate, leading to the conversion of $Na_{1.95}Al_{1.95}Si_{0.05}O_4$ back into $Na_{1.75}Al_{1.75}Si_{0.25}O_4$. Sun et al. discovered through co-roasting a mixture of diaspore, kaolinite, and sodium carbonate that as the roasting temperature increased to 900–1000 °C, the final product became $Na_{1.95}Al_{1.95}Si_{0.05}O_4$, which exhibited excellent dissolution properties closely resembling those of $NaAlO_2$. Further increasing the roasting temperature led to the formation of $Na_xAl_xSi_{2-x}O_4$ as an intermediate product during the transformation of aluminosilicate into sodium aluminate. The solubility of $Na_xAl_xSi_{2-x}O_4$ gradually increased with the rise of the x parameter [16, 17]. Under the condition of a roasting temperature of 750 °C with other variables held constant, the influence of roasting time on the mineral phase evolution of the roasted products was investigated. The results indicate that when the roasting time was extended from 60 to 120 min, the mineral phase composition and content of the roasted products showed no significant changes, suggesting that the reaction had essentially reached completion by this stage.

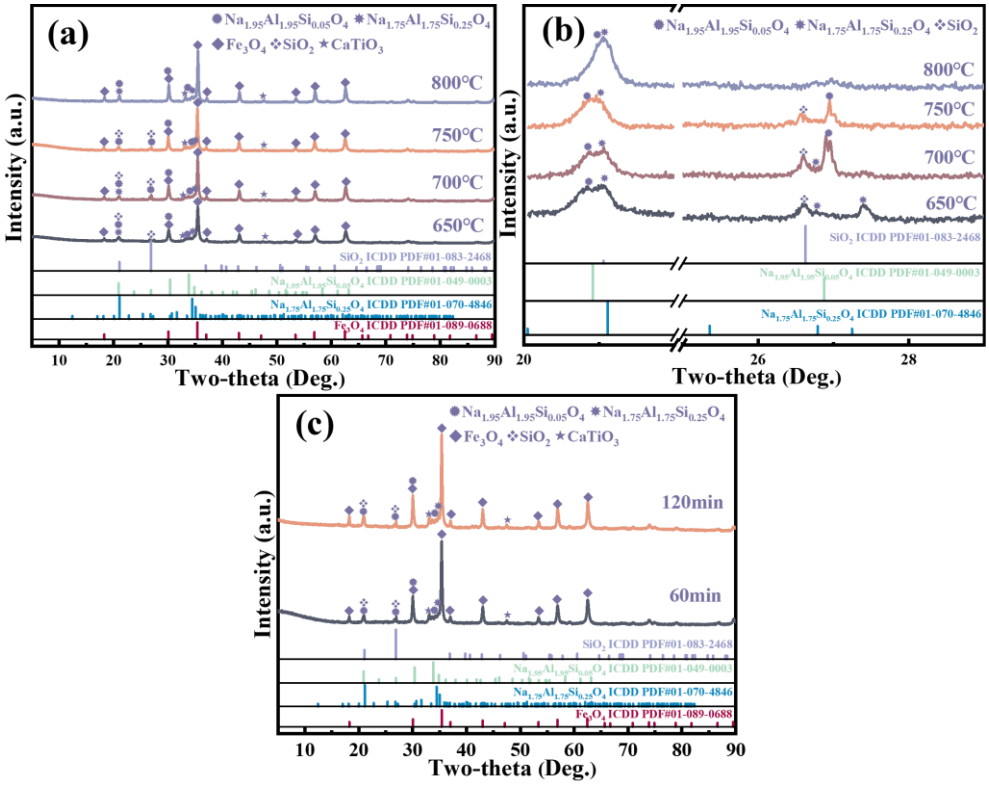

Figure 1. XRD patterns of products obtained under different roasting conditions. (a, b) Roasting temperature, (c) Roasting time.

Table 2. Mineral phase composition of products under different roasting conditions (%).

Roasting temperature (℃)	Roasting time (min)	Fe_3O_4	$Na_{1.75}Al_{1.75}Si_{0.25}O_4$	$Na_{1.95}Al_{1.95}Si_{0.05}O_4$	SiO_2
650	60	51.9	33.4	6.4	2.6
700	60	52.2	18.6	21.6	2.5
750	60	52.8	8.6	32.1	2.5
	120	53.0	8.2	32.6	2.4
800	60	53.1	17.5	21.9	-

Figure 2 illustrates the variations in metal recovery performance under different roasting temperatures and durations. As the roasting temperature increases, the recovery rate of Na_2O remains relatively stable, while that of Al_2O_3 initially rises and then stabilizes, reaching a maximum of 81.56 % at 750 °C. This is attributed to the temperature-induced transformation of $Na_{1.75}Al_{1.75}Si_{0.25}O_4$ into $Na_{1.95}Al_{1.95}Si_{0.05}O_4$, thereby enhancing the recovery of Al_2O_3. The TFe content in the iron concentrate increases with rising temperature before slightly decreasing. While the Al_2O_3 content has an opposite trend, both the yield and iron recovery rate initially rise with increasing temperature before stabilizing. As the roasting time prolongs, the Na_2O recovery rate shows no significant change, whereas the Al_2O_3 recovery rate first increases and then remains unchanged. The TFe content in the iron concentrate follows a similar pattern to the Al_2O_3 recovery rate. In contrast, the yield and iron recovery rate first improve markedly before declining gradually. Based on the above results, the optimal roasting temperature and time should be selected as 750 °C and 60 min, respectively. Under these conditions, the yield and iron recovery rate of the iron concentrate reach 90.59 % and 92.62 %, respectively, while the TFe, Al_2O_3, and Na_2O contents in the iron concentrate are 54.75 %, 4.10 %, and 0.95 %, respectively.

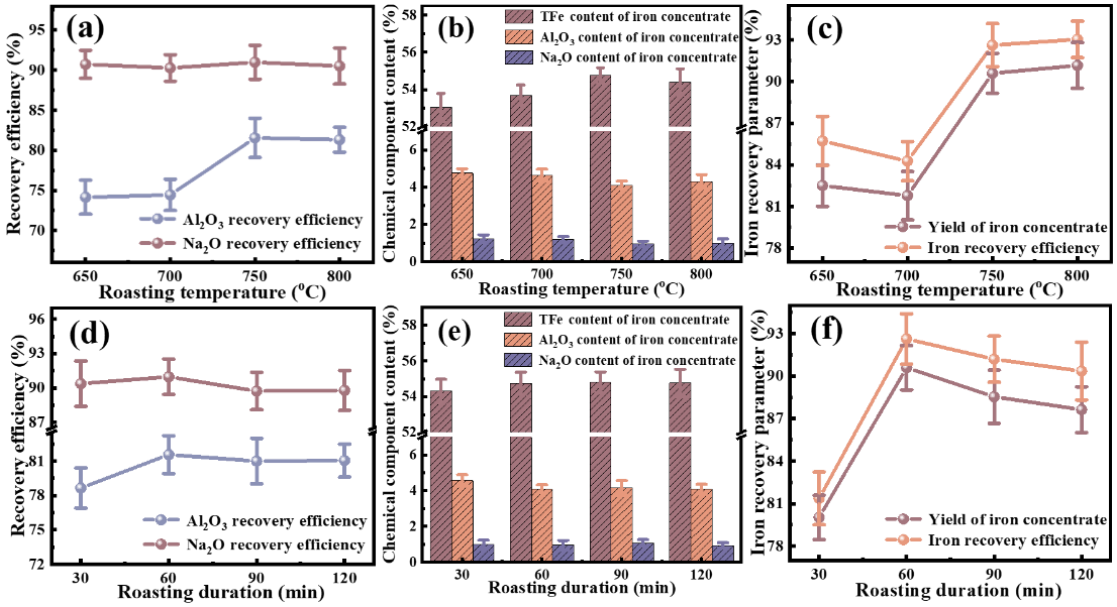

Figure 2. Iron and alumina recovery performance under different roasting conditions. (a, d) Leaching rates of Al_2O_3 and Na_2O, (b, e) Chemical composition of iron concentrate, (c, f) Grade and iron recovery rate of iron concentrate.

3.2 Influence of Batching Ratio Conditions on Mineral Phase Transformation and Recovery Performance of Valuable Elements

Under the optimal roasting conditions, the influence of the N/A and C/O molar ratio in the mixed raw materials on the mineral phase evolution of the sintered products was further investigated. The XRD analysis results of the roasted products are shown in Figure 3. When the C/O molar ratio increased from 0.3 to 0.4, the diffraction peak intensity of Fe_3O_4 decreased while FeO diffraction peaks appeared. This indicates that excess coal reduced Fe_3O_4 to FeO, leading to decreased magnetism of the roasted products and consequently lowering iron recovery.

From Figure 3(b), it can be observed that when the molar ratio of Na/A is 1.0, the main phases of the roasted products are $Na_{1.95}Al_{1.95}Si_{0.05}O_4$, $Na_{1.75}Al_{1.75}Si_{0.25}O_4$, Fe_3O_4, SiO_2, and $CaTiO_3$. As the N/A molar ratio increases to 1.4, the diffraction peak intensity of $Na_{1.75}Al_{1.75}Si_{0.25}O_4$ decreases, while that of $Na_{1.95}Al_{1.95}Si_{0.05}O_4$ increases, indicating that higher NaOH dosage promotes the formation of soluble sodium aluminosilicate. With the increase of the N/A molar ratio to 1.8, the diffraction peak intensity of Fe_3O_4 significantly decreased, while the diffraction peaks of FeO and $NaFe_{0.75}Al_{0.25}O_2$ emerged and gradually intensified. This indicates that further elevation of the N/A molar ratio could hardly promote the transformation of $Na_{1.75}Al_{1.75}Si_{0.25}O_4$ into $Na_{1.95}Al_{1.95}Si_{0.05}O_4$ but instead precipitated Fe_3O_4 into weakly magnetic FeO and $NaFe_{0.75}Al_{0.25}O_2$, consequently leading to a decline in iron recovery rate.

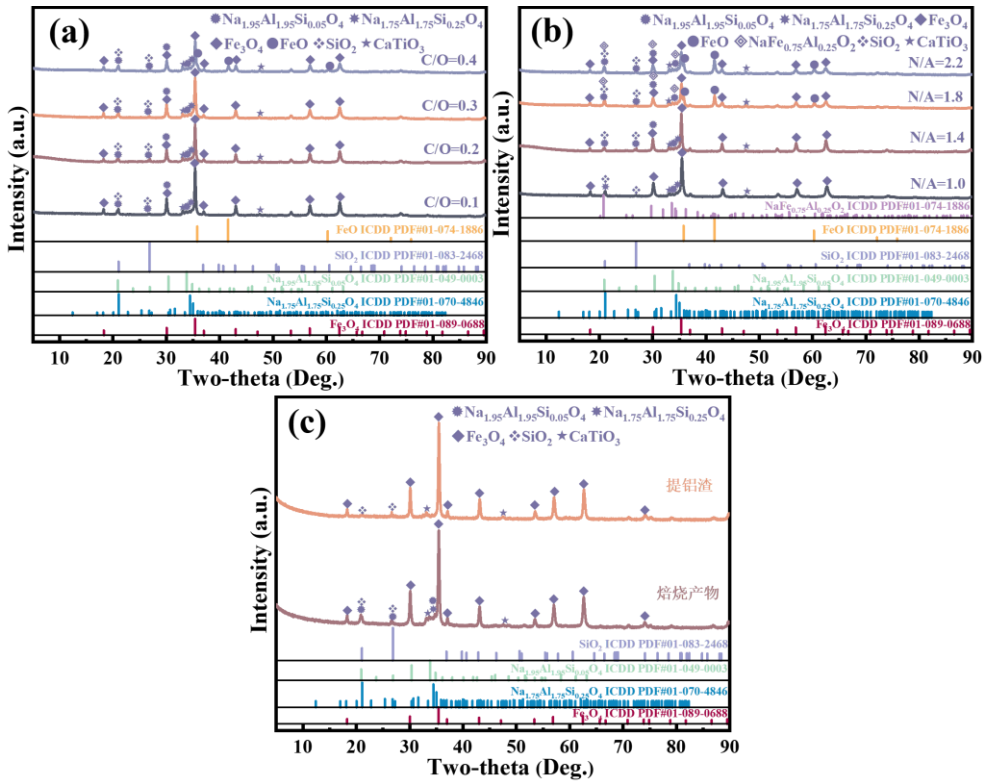

Fig. 3. XRD patterns of products under different batching ratio conditions. (a) C/O molar ratio, (b) N/A molar ratio, (c) roasted products and alumina-extracted residues.

Table 3. Mineral phase composition of products under different batching ratio conditions (%).

C/O	N/A	Fe_3O_4	FeO	$NaFe_{0.75}Al_{0.25}O_2$	$Na_{1.95}Al_{1.95}Si_{0.05}O_4$	$Na_{1.75}Al_{1.75}Si_{0.25}O_4$	SiO_2
0.1	1.4	50.8	-	-	32.2	8.4	2.5
0.2	1.0	50.8	-	-	24.2	17.5	2.5
	1.4	52.8	-	-	32.1	8.6	2.5
	1.8	42.3	4.4	6.5	38.7	-	2.4
	2.0	38.2	6.7	8.8	39.2	-	2.3
0.3	1.4	52.5	-	-	32.3	8.8	2.6
0.4	1.4	45.6	6.2	-	32.7	8.7	2.6

Figure 4 illustrates the variations in metal recovery performance under different C/O and N/A molar ratios. As the C/O molar ratio increases, the recovery rate of Na_2O remains constant, while that of Al_2O_3 shows a slight increase before stabilizing. The chemical composition of the iron concentrate has no significant changes, with its yield and iron recovery rate initially improving but subsequently decreasing markedly. This is attributed to excessive coal powder promoting the formation of FeO, thereby reducing the magnetism of the roasted products. When the N/A molar ratio increased from 1.0 to 1.4, the recovery rate of Na_2O first rose and then declined, while the recovery rate of Al_2O_3 increased significantly before gradually stabilizing. This is because the increase in the N/A molar ratio promoted the transformation of $Na_{1.75}Al_{1.75}Si_{0.25}O_4$ into $Na_{1.95}Al_{1.95}Si_{0.05}O_4$. When the N/A molar ratio exceeds 1.8, Fe_3O_4 precipitates into FeO and $NaFe_{0.75}Al_{0.25}O_2$, where $NaFe_{0.75}Al_{0.25}O_2$ acts as a weakly magnetic insoluble phase, significantly reducing the efficiency of iron-alumina separation and recovery. The TFe content in the iron concentrate continuously increases with the rising N/A molar ratio, while the Al_2O_3 content shows an opposite trend, corresponding to the variation in Al_2O_3 recovery rate. This indicates that an

increased N/A molar ratio promotes the dissociation of iron and aluminium elements in bauxite residue. The yield of iron concentrate and iron recovery rate initially increase and then decrease with the rising N/A molar ratio, which can be attributed to the disruption of Fe-Al lattice substitution and the formation of $NaFe_{0.75}Al_{0.25}O_2$. Based on these results, the optimal C/O and N/A molar ratios are determined to be 0.2 and 1.4, respectively.

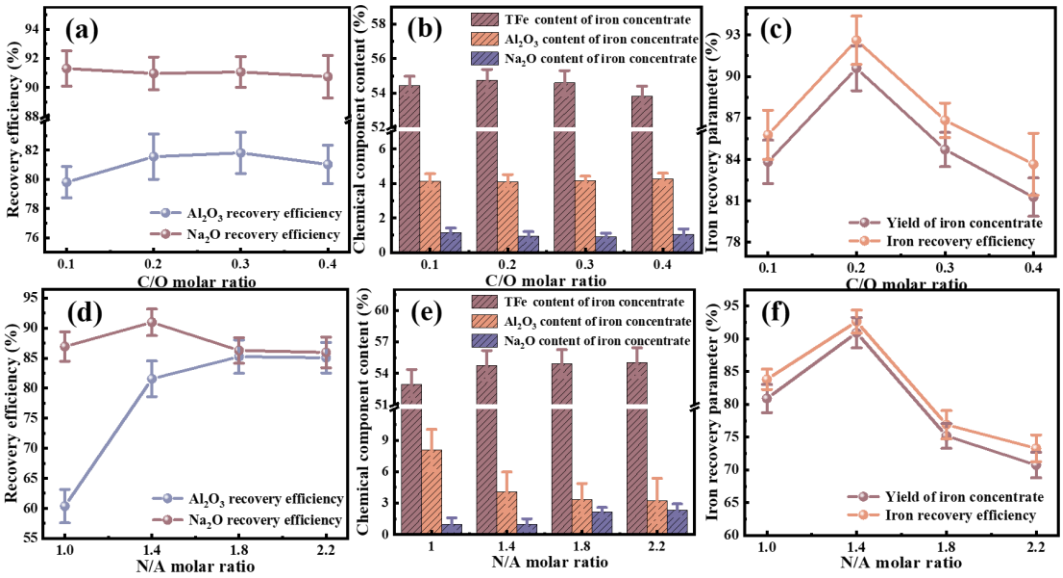

Figure 4. Iron and alumina recovery performance under different batching ratio conditions. (a, d) Leaching rates of Al_2O_3 and Na_2O, (b, e) Chemical composition of iron concentrate, (c, f) Grade and iron recovery rate of iron concentrate.

To further purify and upgrade the magnetic separation product (iron concentrate), the impacts of alumina-extracted residue particle size and magnetic field intensity on the magnetic separation of iron concentrate were investigated under optimal roasting and batching ratio conditions. Figure 5a shows the particle size distribution of alumina-extracted residue under different grinding durations, with median particle sizes D_{50} of 16.31, 10.92, 10.65, 9.26, and 3.95 μm, respectively. The TFe content of the iron concentrate initially increases and then decreases with the reduction of particle size of alumina-extracted residue, while both the yield and iron recovery rate consistently decline. This is attributed to the further separation of magnetic and non-magnetic minerals through grinding. However, excessively fine particles may cause the alumina-extracted residue to become muddy, thereby deteriorating the efficiency of magnetic separation. As a result, a portion of the gangue minerals is entrained into the iron concentrate during magnetic separation, while the remainder becomes concentrated in the iron-extracted tailings. The TFe content of iron concentrate decreases with increasing magnetic field intensity, while its yield and iron recovery rate show the opposite trend. This is because a stronger magnetic field captures more weakly magnetic minerals, thereby recovering more iron resources, but it also reduces the purity of the iron concentrate. Therefore, the magnetic field intensity for low-intensity magnetic separation should not be set too high. Based on the above analysis, the optimal grinding time and magnetic field intensity are determined to be 10 min (with a D_{50} of 10.92 μm) and 1650 Oe, respectively. Under these conditions, the TFe, Al_2O_3, and Na_2O contents of the iron concentrate reach 55.21 %, 3.87 %, and 0.82 %, while the corresponding yield and iron recovery rate are 87.97 % and 90.37 %, respectively.

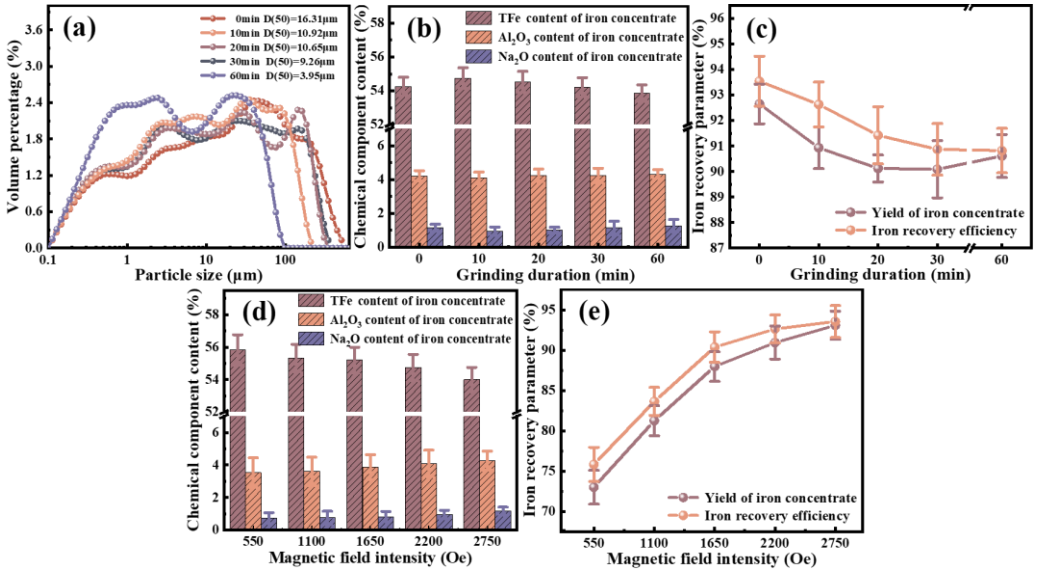

Figure 5. Iron recovery performance under different magnetic separation conditions. (a) Particle size of alumina-extracted residue; (b, d) chemical composition of iron concentrate; (c, e) grade and iron recovery rate of iron concentrate.

3.3 Study on Reaction Mechanism of Soda-magnetization Reduction Roasting

To analyse the iron phase composition in the roasted products, the Mössbauer spectrum of the roasted products obtained under optimal roasting conditions is shown in Figure 6a. The original experimental data were fitted to two sextets and one doublet sub-spectra. The isomer shifts (IS) of the Fe_3O_4 (A) and Fe_3O_4 (B) sextets were 0.32 and 0.66 mm/s, respectively, accounting for 92 % of the total mineral content. This indicates that nearly all iron minerals in the roasted products were present as Fe_3O_4. Additionally, the IS and quadrupole splitting (QS) of the coordinated Fe^{3+} were 0.28 and 0.79 mm/s, respectively, with a corresponding spectral area of 8 %. This spectrum is associated with Fe^{3+} and Al^{3+} coordinated in aluminosilicate structures, likely due to the substitution of iron and aluminium elements in sodium aluminosilicate [18, 19].

As shown in Figures 6b–6e, XPS was employed to investigate the variation of surface atomic valence states at different stages. Both bauxite residue and roasted products contained Na, Fe, O, Ti, Ca, Si, and Al elements. Notably, the disappearance of the Na peak in alumina-extracted residue was accompanied by a reduction in Al peak intensity, which can be attributed to the effective dissolution of sodium aluminosilicate compounds. The contents of $[AlO_4]$ and $[AlO_6]$ in the roasted product are 71.18 % and 28.82 %, respectively, while those in the alumina-extracted residue are 66.67 % and 33.33 %, respectively. It can be concluded that the soda leaching process removed $Na_{1.75}Al_{1.75}Si_{0.25}O_4$ and $Na_{1.95}Al_{1.95}Si_{0.05}O_4$ (composed of $[AlO_4]$) from the roasted product. The Fe2p spectrum of bauxite residue has four peaks, including $Fe2p_{3/2}$, $Fe2p_{1/2}$, $Fe2p_{3/2}$ satellite peak, and $Fe2p_{1/2}$ satellite peak. The $Fe2p_{3/2}$ and $Fe2p_{1/2}$ peaks are entirely composed of Fe^{3+}, corresponding to goethite and hematite in the bauxite residue. The appearance of the Fe^{2+} peak caused the $Fe2p_{3/2}$ and $Fe2p_{1/2}$ peaks of the roasted product to shift from 711.12 eV and 724.92 eV to 710.64 eV and 724.84 eV, respectively, indicating the transformation of iron oxides in bauxite residue into magnetite. For the alumina-extracted residue, the $Fe2p_{3/2}$ and $Fe2p_{1/2}$ peaks shifted to lower binding energies at 710.72 eV and 724.88 eV, respectively, due to the enhanced intensity of the Fe^{3+} peak, suggesting that the dissolution of sodium aluminosilicate compounds promoted the dissociation of iron-aluminium minerals in the roasted products. In the case of the iron concentrate, the $Fe2p_{3/2}$ and $Fe2p_{1/2}$ peaks shifted to higher binding energies at 710.41 eV and 724.59 eV, respectively, which was attributed to the incomplete reduction of dissociated Fe^{3+} and its subsequent separation into tailings, leading to an increased intensity of the Fe^{2+} peak.

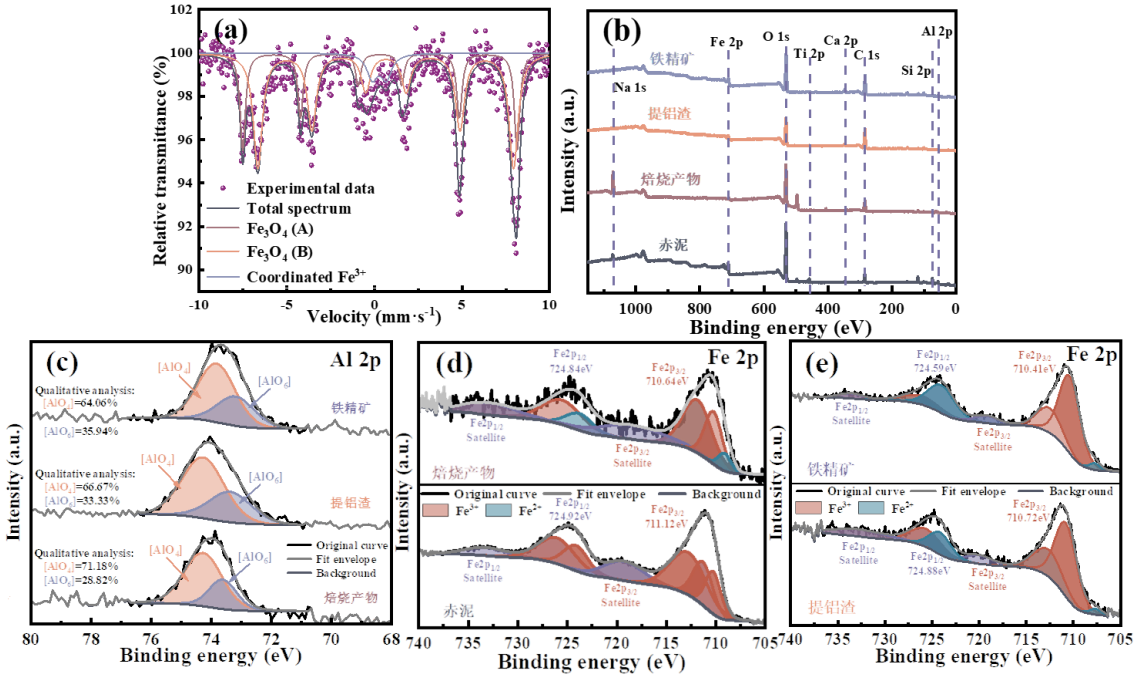

Figure 6. Mossbauer spectrum and XPS analysis patterns of the product obtained under optimal conditions. (a) Mossbauer spectrum of the roasted products, (b) XPS full spectrum, (c) Al 2p high-resolution spectrum, (d, e) Fe 2p high-resolution spectra.

To reveal the recovery mechanism of iron and alumina resources from bauxite residue during soda-magnetization roasting from a microscopic perspective, the micro-morphology and elemental distribution of roasted products and alumina-extracted residues under optimal experimental conditions were analysed using SEM-EDS. As shown in Figures 7a–7d, the roasted products consist of sodium aluminosilicate, magnetite, perovskite, and rutile. The elements Na, Al, Si, and O are tightly bound in the form of sodium aluminosilicate, while an independent quartz phase can also be observed in the Si elemental mapping. Additionally, the Ti element distribution map indicates that Ti and Ca exist in the form of perovskite, and independent rutile can be observed. Figures 7e–7h indicate that the spherical minerals in the alumina-extracted residue are primarily magnetite with minor impurity elements. The minerals at points B and C consist of magnetite, perovskite, alumina, and rutile, while the mineral composition at point D is similar to that at point A. The main magnetic mineral in alumina-extracted residue is magnetite, which can be recovered by magnetic separation as a strongly magnetic mineral. Other non-magnetic minerals such as perovskite, rutile, and quartz are separated during magnetic separation and concentrated into the iron-extracted tailings.

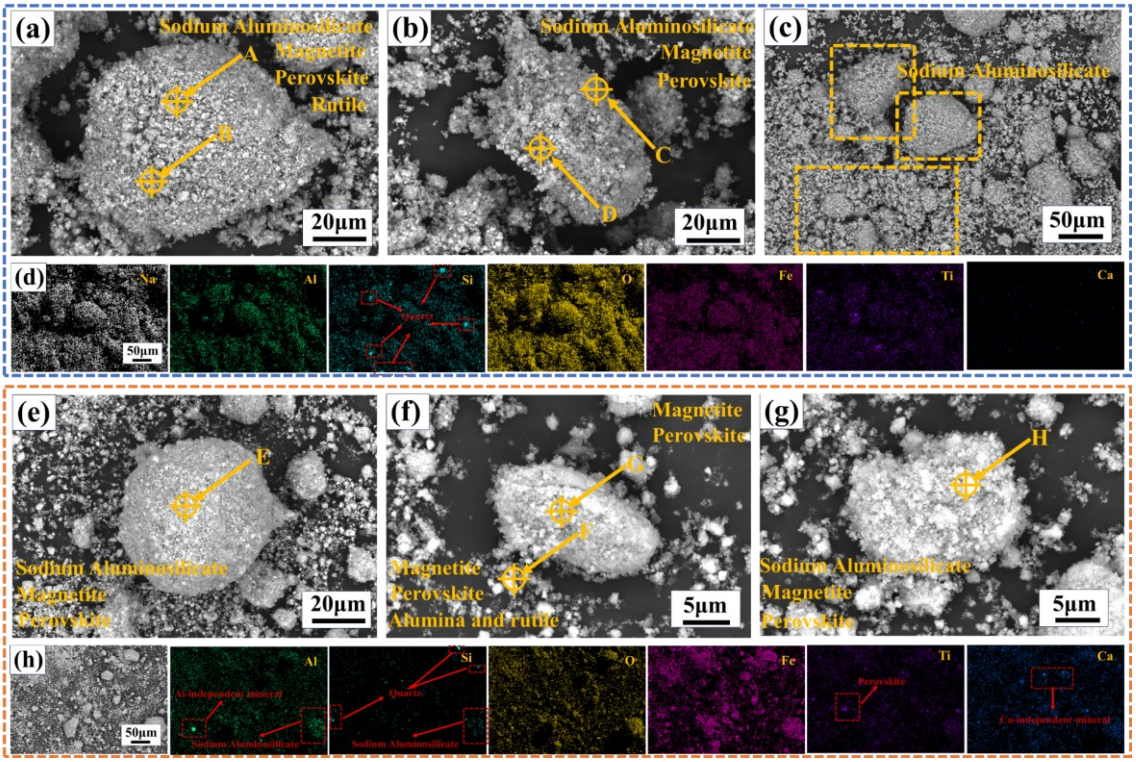

Figure 7. Micro-morphology and elemental distribution of samples under optimal conditions. (a-d) Roasted products, (e-h) Alumina-extracted residue.

Table 4. EDS analysis results (wt.%).

Measurement point	O	Fe	Al	Na	Si	Ti	Ca
A	62.32	12.59	7.83	13.23	2.29	0.97	0.78
B	41.82	48.32	3.41	4.71	0.77	0.97	-
C	64.60	6.93	10.34	14.87	1.84	0.82	0.60
D	56.92	14.63	10.28	14.11	2.62	0.88	0.56
E	67.93	21.44	3.10	1.02	2.92	1.80	1.80
F	21.46	73.74	1.02	-	-	2.56	1.22
G	64.07	32.32	1.10	-	0.82	0.98	0.70
H	69.14	25.13	2.07	1.18	1.45	0.53	0.50

Based on the above results and discussion, Figure 8 summarizes the mineral transformation mechanisms of iron oxides and sodium aluminosilicate during the soda-magnetization reduction process. With increasing roasting temperature and C/O molar ratio, FeOOH undergoes dehydration and converts to Fe_3O_4 together with Fe_2O_3. When the C/O molar ratio reaches 0.3, Fe_3O_4 becomes excessively reduced to FeO. Similarly, excessive increase in the N/A molar ratio causes sodium incorporation into Fe_3O_4, subsequently precipitating into FeO and $NaFe_{0.75}Al_{0.25}O_2$, ultimately leading to decreased iron recovery efficiency. During the magnetization reduction roasting process, hydrated sodium aluminosilicate dehydrates to form $NaAlSiO_4$, which subsequently reacts with NaOH to gradually transform into soluble sodium aluminosilicates ($Na_{1.75}Al_{1.75}Si_{0.25}O_4$ and $Na_{1.95}Al_{1.95}Si_{0.05}O_4$). When the temperature exceeds 750 °C, SiO_2 participates in the reaction and converts $Na_{1.95}Al_{1.95}Si_{0.05}O_4$ into $Na_{1.75}Al_{1.75}Si_{0.25}O_4$. This leads to more impurity SiO_2 entering the leaching liquor. Although these impurities are removed in subsequent processing, they also carry away Al_2O_3 from the liquor, thereby reducing the overall

efficiency of the process. Based on the material balance calculation results, it can be observed that for each tonne of bauxite residue, after adding the optimal proportion of coal and soda liquor and undergoing roasting, 0.92 tonnes of roasted product is obtained. Through dilute soda atmospheric pressure leaching, 0.61 tonnes of leached residue can be obtained, during which most of the alumina and sodium oxide resources can be recovered. The leached residue yields 0.54 tonnes of iron concentrate and 0.07 tonnes of magnetic separation tailings after magnetic separation. Calculations indicate that the comprehensive reduction rate of bauxite residue through this process is approximately 93 % when comparing the mass of bauxite residue before treatment and the tailings after treatment. Moreover, the Na, Al, and Si elements in bauxite residue are the primary components for synthesizing geopolymers, particularly after roasting activation [20]. The sodium aluminosilicate in tailings can serve as a precursor for geopolymer synthesis, where the Si-O and Al-O bonds break under soda conditions and reorganize into [AlO_4] and [SiO_4] tetrahedra. Therefore, the iron-separated tailings in this study can be regarded as high-quality raw materials for producing green high-strength geopolymer construction materials [21, 22].

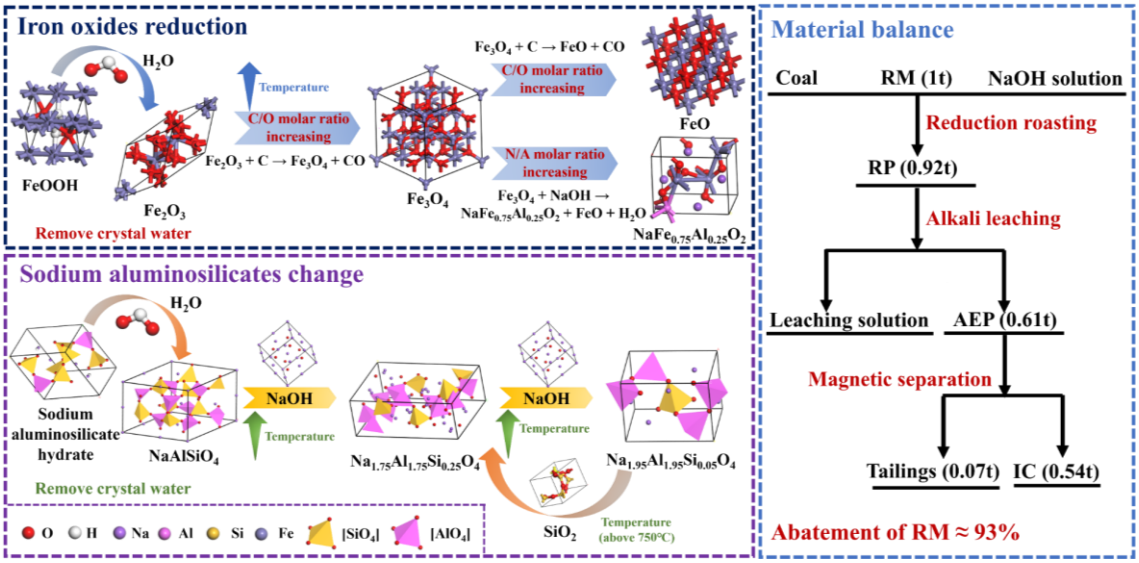

Figure 8. Schematic diagram of the reaction mechanism for soda-magnetization reduction roasting.

4. Conclusion

(1) The increase in roasting temperature and N/A molar ratio promoted the transformation of $Na_{1.75}Al_{1.75}Si_{0.25}O_4$ into $Na_{1.95}Al_{1.95}Si_{0.05}O_4$. When the temperature exceeded 750 °C, SiO_2 induced the conversion of $Na_{1.75}Al_{1.75}Si_{0.25}O_4$ back into $Na_{1.75}Al_{1.75}Si_{0.25}O_4$. Excessive C/O and N/A molar ratios led to the over-reduction and sodiation of Fe_3O_4, forming weakly magnetic FeO and $NaFe_{0.75}Al_{0.25}O_2$, thereby reducing the magnetism of the roasted product and deteriorating iron recovery efficiency.

(2) The optimal process conditions for the soda-magnetization reduction recovery of iron and alumina resources from bauxite residue are as follows: a roasting temperature of 750 °C, roasting time of 60 min, C/O and N/A molar ratios of 0.2 and 1.4, grinding time of 10 min, and magnetic field intensity of 1650 Oe. Under these conditions, the recovery rates of Al_2O_3 and Na_2O in the roasted product are 81.56 % and 90.97 %, respectively. The iron concentrate contains 55.21 % TFe, 3.87 % Al_2O_3, and 0.82 % Na_2O, with a yield of 87.97 % and an iron recovery rate of 90.37 %.

(3) Over 92 % of the iron minerals in the roasted product are strongly magnetic magnetite. Among them, $Na_{1.75}Al_{1.75}Si_{0.25}O_4$ and $Na_{1.95}Al_{1.95}Si_{0.05}O_4$ are recovered via atmospheric leaching, achieving a comprehensive reduction rate of bauxite residue exceeding 93 %. The sodium aluminosilicate in the tailings has strong cementitious reactivity and can be used as a raw material for producing geopolymer-based green building materials, thereby enabling the full-scale and efficient utilization of bauxite residue.

5. References

1. Xin Huang, et al., Research progress on bauxite residue utilization and radioactivity studies [J], *Recyclable Resources and Circular Economy*, 2025, 18(03): 25–31 (in Chinese).
2. X Y Li, et al., Synthesis process-based mechanical property optimization of alkali-activated materials from red mud: A review[J], Journal of environmental management, 2023, 344: 118616.
3. Xiaolin Pan, et al., Research status and prospects of iron and aluminum recovery technology from bauxite residue [J], *The Chinese Journal of Nonferrous Metals*, 2023, 33(11): 3879–3899 (in Chinese).
4. X L Pan, et al., Recovery of valuable metals from red mud: A comprehensive review[J], *Science of The Total Environment*, 2023, 904(15): 166686.
5. R A Pepper, et al., Value adding red mud waste: Impact of red mud composition upon fluoride removal performance of synthesised akaganeite sorbents[J], *Journal of Environmental Chemical Engineering,* 2018, 6(2): 2063–2074.
6. P K Liu, et al., The separation performance of a parabolic hydrocyclone in separating iron from red mud[J], *Powder Technology*, 2023, 416(15): 118205.
7. X B Zhu, et al., A novel process for recovery of aluminum, iron, vanadium, scandium, titanium and silicon from red mud[J], *Journal of Environmental Chemical Engineering*, 2020, 8(2): 103528.
8. Z Karami, A Rahbar-Kelishami, The Study of Acid Leaching on the Mineralogical and Microscopic Changes of Red Mud[J], Mining, Metallurgy & Exploration, 2024, 41: 1121–1133.
9. Q Y Lei, et al., Separation and recovery of scandium and titanium from red mud leaching liquor through a neutralization precipitation-acid leaching approach[J], *Journal of Rare Earths*, 2021, 39(9): 1126–1132.
10. Taotao Sun, et al., Research progress on iron extraction from bauxite residue[J], *China Nonferrous Metallurgy*, 2024, 53(02): 22–33 (in Chinese).
11. H M Wang, et al., Transformation Behavior of Iron Minerals in High-Iron Red Mud During High-Pressure Hydrothermal Reduction[J], *Bulletin of Environmental Contamination and Toxicology*, 2022, 109: 76–85.
12. P F Wu, et al., The harmless and value-added utilization of red mud: Recovering iron from red mud by pyrometallurgy and preparing cementitious materials with its tailings[J], *Journal of Industrial and Engineering Chemistry*, 2024, 132(25): 50–65.
13. Y Wu, et al., Recovery of Iron and Alumina from Iron-Rich Bauxite, Red Mud, and Fly Ash by Reduction Smelting with Steel Slag[J], JOM, 2024, 76: 2457–2467.
14. S Yuan, et al., A semi-industrial experiment of suspension magnetization roasting technology for separation of iron minerals from red mud[J], *Journal of Hazardous Materials*, 2020, 394(15): 122579.
15. Yingjie Shi, et al., Engineering application and economic analysis of iron recovery from bauxite residue by magnetizing roasting [J], *Nonferrous Metals Engineering*, 2024, 51(03): 41–46 (in Chinese).
16. J H Zhang, et al., Recovery of iron and alumina from iron-aluminum symbiotic ore via low-calcium carbothermal reduction[J], Minerals Engineering, 2023, 204: 108426.
17. Y Sun, et al., Activation mechanism of diasporic bauxite calcined with sodium carbonate[J], *Minerals Engineering*, 2022, 187: 107782.

18. X Liu, et al., Clean utilization of high-iron red mud by suspension magnetization roasting[J], *Minerals Engineering*, 2020, 157(01): 106553.
19. N Ye, et al., Transformations of Na, Al, Si and Fe species in red mud during synthesis of one-part geopolymers[J], *Cement and Concrete Research*, 2017, 101: 123–130.
20. P N Lemougna, et al., Synthesis and characterization of low temperature (< 800 ºC) ceramics from red mud geopolymer precursor[J], *Construction and Building Materials*, 2017, 131(30): 564–573.
21. Y Hu, et al., Role of Fe species in geopolymer synthesized from alkali-thermal pretreated Fe-rich Bayer red mud[J], *Construction and Building Materials*, 2019, 200(10): 398–407.
22. N Shehata, et al., Recent progress in environmentally friendly geopolymers: A review[J], *Science of The Total Environment,* 2021,762(25): 143166.